DEMOSAICING STRATEGY IDENTIFICATION VIA EIGENALGORITHMS

Simone Milani, Paolo Bestagini, Marco Tagliasacchi, Stefano Tubaro

Dipartimento di Elettronica, Informazione, e Bioingegneria - Politecnico di Milano,
e-mail: {milani,bestagini}@elet.polimi.it,{marco.tagliasacchi,stefano.tubaro}@polimi.it

ABSTRACT

The identification of the camera that has acquired a specific image can be performed via several device-related footprints. Among these, it is possible to look for the traces left by the adopted color demosaicing strategy, which varies according to the camera model and vendor.

The paper presents an identification strategy that re-processes the analyzed image with a set of distinctive CFA interpolation algorithms (eigenalgorithms) and, according to the correlation of the output with the original image, builds a set of features that permits identifying the algorithm. The proposed solution performs well with respect to other state-of-the-art solutions also when the analyzed image is severely compressed.

Index Terms— demosaicing identification, CFA interpolation, Bayer mask, device identification, image forensics.

1. INTRODUCTION

The identification of the acquisition device is an important clue in the authentication and validation of multimedia content such as images and videos [1].

As for images, several different footprints can be considered as revealing clues useful for the device identification [2]. For example, Photo Response Non Uniformity (PRNU) noise is one of the distinctive feature of the CCD acquisition matrix employed in a camera and, when compression distortion is limited, it permits identifying the originating device [3]. Since most of the images are available in compressed format, several coding artifacts can be detected in an image and used to identify the specific codec implementation since many non-normative aspects are implemented differently by each vendor [4].

In this paper, we focus on the specific Color Filter Array (CFA) interpolation strategy (also known as demosaicing [5]) employed by the camera [6]. In most cameras it is possible to acquire a single color component per pixel, and therefore, color samples are positioned according to a specific acquisition mask (Bayer mask). The missing colors are generated via an interpolation of this mask (before compressing the image), and each camera vendor has developed its own algorithms. Therefore, identifying the demosaicing strategy is an important task in image forensics [7].

Among the possible identification approaches available in the literature [8, 9, 4, 10, 11, **?**], some of the proposed blind techniques rely on the fact that some operators are "idempotent" [12]. This means that, if an operator was used to process the signal under analysis, reprocessing the signal with the same operator will generate output data that proves to be highly-correlated with the analyzed data themselves [13]. Unfortunately, the identification of the demosaicing strategy via idempotence is severely conditioned by image compression level (as it will be shown in Section 4). The performance dramatically collapses whenever lossy compression (e.g., using JPEG) is included in the processing chain. Moreover, idempotence-based detectors imply that the investigated method is included in the analysis set, i.e., an implementation of the demosaicing strategy to be identified is available to the analyst. This assumption might not be true in practice.

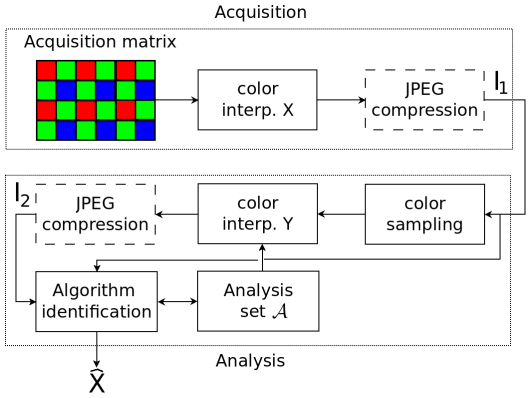

Fig. 1. Processing and analysis chain using idempotence property.

In this paper, we try to identify the demosaicing strategy by analyzing the interpolated image via eigenalgorithms [14]. The analyzed image is re-processed with a set of distinctive strategies (called *eigenalgorithms*), which enable to characterize it in an "eigen-correlation" space. The position assumed in the space is a revealing trace of the specific demosaicing approach. The proposed solution permits a correct identification of the interpolation strategy even in the presence of lossy JPEG compression, and does not imply that the algorithm to be identified must be available to the analyst. Experimental results show that the proposed analysis technique can be applied to images taken by consumer cameras and leads to their correct identification. In the following, Section 2 describes the idempotence property, while Section 3 extends this concept introducing eigenalgorithms. Section 4 reports the detection performance and Section 5 draws the final conclusions.

2. THE IDEMPOTENCE PRINCIPLE

A conceptual illustration of the proposed identification scheme based on the idempotent property is presented in Fig. 1. Let I_1 denote the image under analysis, which is the result of processing the acquired color samples with the unknown algorithm X. The analyst has a set of processing units $Y \in \mathcal{A}$ at hand. For each of them, he generates

The project REWIND acknowledges the financial support of the Future and Emerging Technologies (FET) programme within the Seventh Framework Programme for Research of the European Commission, under FET-Open grant number:268478.

the output data I_2 by resampling I_1 according to the Bayer mask and interpolating it with algorithm Y.

The correlation between I_2 and I_1 is a distinctive feature of the unknown algorithm X. In this research work, it is measured via the PSNR value between pixels of I_1 and I_2. Assuming that I_2 was obtained using the algorithm Y, the PSNR value between I_1 and I_2 is p_Y.

The demosaicing strategy that leads to the highest PSNR is identified with the unknown strategy X, i.e.,

$$\hat{X} = \arg\max_{Y \in \mathcal{A}} p_Y \tag{1}$$

In the literature, the idempotent property has been successfully exploited for the identification of the quantizer [15], the traces left by JPEG compression antiforensics [16], and the adopted video coding architecture [12, 17].

Experimental results in Section 4 will show that when dealing with CA interpolation strategy detection, the performance is severely conditioned by compression artifacts. Moreover, the set $\mathcal{A}$ must include strategy X to be identified; otherwise, it is only possible to identify the algorithm in $\mathcal{A}$ that is the closest to X (but does not necessarily correspond to X). The proposed method, presented in the next section, is able to circumvent these shortcomings.

3. INTERPOLATION STRATEGY IDENTIFICATION VIA EIGENALGORITHMS

Experimental data shows that some of the strategies in $\mathcal{A}$ present different correlation levels with the unknown strategy X. This suggests the idea that it is possible to characterize the unknown interpolation algorithm to be identified via the PSNR values obtained by an adequate set $\mathcal{A}$ of demosaicing solutions (which does not necessarily include the unknown algorithm X). The strategy in this set will be called *eigenalgorithms* (similarly to eigenvector or eigenfunctions) [14].

Given the set of algorithms in Table 1, Fig. 2 reports the PSNR values obtained by processing a set of images I (which has been demosaiced with strategy X) with algorithms A, B, and C. The possible interpolators X are reported in Table 1. Results are plotted in a couple of graph displaying p_A vs. p_B and p_B vs. p_C. Note that since no compression was performed, $p_X \to +\infty$ (with $X = A, B, C$) since the mentioned strategies do not alter the acquired reference color samples. In order to allow a better visualization and computation, values $p_X = +\infty$ are replaced with $p_X = 60$ dB. It is possible to notice that points

$$\overline{p} = (p_A, p_B, p_C) \tag{2}$$

related to a specific algorithm X occupy a definite region R_X in the three-dimensional feature space (for the sake of clarity, this feature space is split into two 2-D plots in Fig. 2).

Similar results were obtained when the image was compressed.[1] Figure 3 reports the points (p_A, p_B, p_C) obtained from JPEG images coded with QF=85.

In the following, it will be explained how to characterize the decision regions R_X and determine the interpolation strategy given the input vector $\overline{p}$. More precisely, we distinguished two experimental settings. A first setting consists in a controlled scenario where the whole chain (acquisition,demosaicing,compression) is simulated and all the processing steps are known. A second setting considers images taken by different commercial cameras. In the first case regions of $\overline{p}$ that characterize each algorithm are more regular, while

[1] In this work, we will consider JPEG compression.

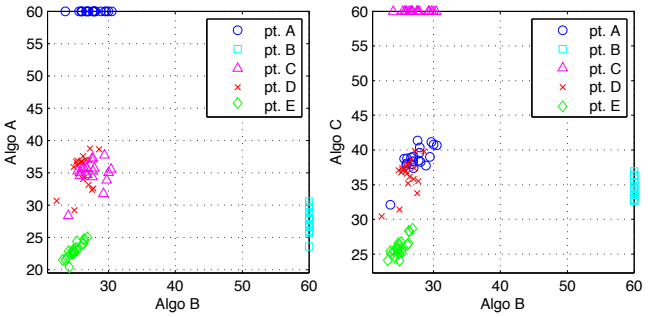

(a) (b)

Fig. 2. Diagrams of points $\mathbf{p} = (p_A, p_B)$ and $\mathbf{p} = (p_C, p_B)$ for different demosaicing algorithms. Points labelled `pts X` denotes values $\mathbf{p}$ related to unknown algorithm X. Points belonging to different algorithms cluster in regions R_X. a) Points $\mathbf{p} = (p_A, p_B)$ b) Points $\mathbf{p} = (p_C, p_B)$.

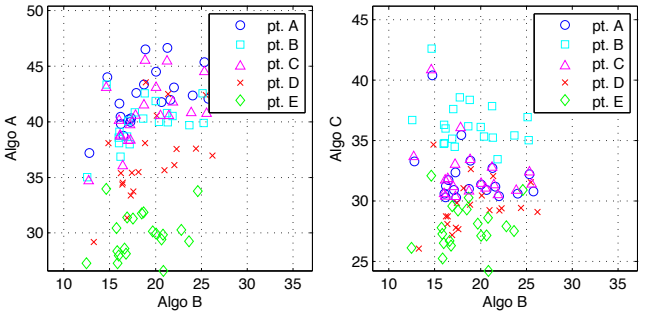

(a) (b)

Fig. 3. Diagrams of points $\mathbf{p} = (p_A, p_B)$ and $\mathbf{p} = (p_C, p_B)$ for different demosaicing algorithms on compressed images. For the sake of conciseness, the convention of notation is the same of Fig. 2. The JPEG quality factor of images is 85. a) Points $\mathbf{p} = (p_A, p_B)$ b) Points $\mathbf{p} = (p_C, p_B)$.

in the latter, regions have more complex shapes. This fact is mainly due to the influence of other processing units (like white-balancing, gamma correction, compression, rate-distortion optimization, etc..) on the final images. Therefore, the regions R_X can be correctly characterized by training a set of classifiers based on a Support Vector Machine (SVM) [18].

The vectors $\overline{p}$ related to a specific image is fed to a set of binary SVM classifiers that report whether the processed image has to be related to a specific strategy Y, i.e., each classifier tries to state whether $\overline{p}$ refers to $Y \in \mathcal{A}$ or not. Each classifier (associated to the algorithm/camera Y) outputs a real value $w_Y \gtrless 0$, whose absolute value corresponds to the distance from the separating hyperplane.

Combining the outputs of the different classifiers in the variables

$$W_Y = w_Y - \sum_{Z \in \mathcal{A}; Z \neq Y} w_Z, \tag{3}$$

where signs are combined according to the algorithm we are considering, it is possible to estimate the adopted algorithm via the maximum

$$\hat{X} = \arg\max_{Y \in \mathcal{A}} W_Y. \tag{4}$$

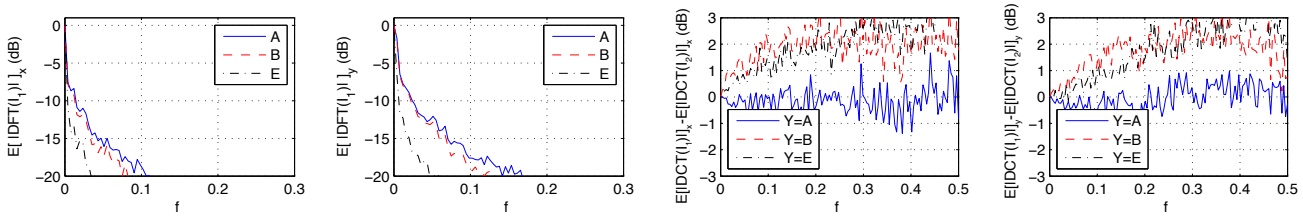

Fig. 4. Fourier transform of image `peppers` sampled and interpolated with different algorithms. Graphs report $|DFT(I_1)|_{dB}$ averaged along columns (a) and rows(b), together with $|DFT(I_1)|_{dB} - |DFT(I_2)|_{dB}$ (with $I_1 = A$) averaged along columns (c) and rows (d). Frequency f is normalized.

A possible explanation for this is provided by Fig. 4, which reports the absolute coefficient values of DFT-transformed image `peppers` averaged along the columns (vertical frequencies) and along the rows (horizontal frequencies). The image has been sampled using RGGB Bayer mask and reinterpolated with algorithms A,B,E. It is possible to notice that the different algorithms differs mostly in processing the input signal in the transient band between low and high frequencies (approximately between 0.07 and 0.1). Low frequency information can be easily estimated by all the proposed solutions. High frequency components prove to be more difficult to reconstruct and different interpolation strategies lead to different amounts of artifacts (e.g., aliasing, rainbows, etc.). In the reported figure, this differentiation is quite evident in the vertical interpolation (Fig. 4b) since the spectra of the three signals are quite separated. As a matter of fact. these differences provide some footprints for the specific interpolation strategy.

These can be acquired by resampling and reinterpolating the image I_1, followed by evaluating the differences with respect to the original data (as described before). From Fig. 4 (c) and (d), it is possible to notice that when the process interpolated with A is reprocessed with E the difference between absolute frequency response is quite close to 1 dB. In case, the process is reprocessed with B the average difference is lower.

4. EXPERIMENTAL RESULTS

In a first set of experiments, we considered the identification of known demosaicing algorithms. To this purpose, images from the UCID dataset [19] were sampled, interpolated, and compressed with different quality factors. In this work we considered the demosaicing strategies reported in Table 1. These strategies were selected since they are clearly described in the literature, results are reproducible, and their performance proves to be quite satisfactory. Moreover, they present a good degree of diversity that makes the different p_Y values more informative with respect to using similar interpolation strategies. This fact was further validated by an extensive set of experiments on the UCID dataset involving a wider set of demosaicing algorithms. Results are omitted here for the sake of conciseness.

The adopted JPEG codec is the one implemented in MATLAB. On the coded images we tested the proposed identification strategy, a detector based on idempotence (i.e., using eq. (1) under the assumption that all the demosaicing strategies are available to the analyst) and that proposed by Gao *et al.* in [20].

In order to evaluate their efficiencies, we tested the detectors in two scenarios. A first scenario considers a set of non compressed images [19], where color components are sampled according to a RGGB Bayer mask, interpolated using one of the algorithms in Table 1, and eventually, compressed (see Fig. 1).

Table 1. Demosaicing strategies

Letter	A	B	C	D	E
Algorithm	DLMMSE	Alternating Projections	hold	bilinear	Self-similarity Driven
Reference	[21]	[22]			[23]

Similarly to the approaches in [24, 20], for every image we select an area of 352×288 pixels (CIF resolution) where the analysis is performed. In our analysis we skipped those blocks with too stationary behavior or too much varying since the outputs of different demosaicing strategy is not discriminative in the first case or significant in the latter (as done in [24]). As a matter of fact, we process the image via a sliding window of CIF resolution computing the average absolute gradients (vertical and horizontal) on the acquired color samples. For every image, we select the CIF window with the highest gradient included in the range 5 and 12. In this way it is possible to identify those parts where the peculiarities of the different interpolation strategies are highlighted. Source code for this selection is available at [25]

Classification is performed considering 3 eigenalgorithms ($\mathcal{A} = \{A, B, C\}$) out of the 5 strategies reported in Table 1. Experimental results have proved that in this controlled experimental setting, 3 strategies were enough to identify all 5 techniques. Note that the implementations of algorithms D and E were not available to the analyst. Additional results have shown that increasing the number of cameras/algorithms to be detected imply increasing the number of features/algorithms to be used in the generation of $\overline{p}$. Moreover, the outputs of the analysis algorithms A, B, C must be uncorrelated to permit an accurate classification. In the presented results, we processed a common set of training images with different algorithms and we computed the correlation between the different outputs. Algorithms A, B, C were selected maximizing the uncorrelation levels between the different outputs.

Fig. 5 reports the detection accuracies for the different methods and quality factors QF. It is possible to see that the proposed strategy is quite robust with respect to the distortion introduced by compression. It is possible to notice that in case no strong compression is perform on the images, all the solutions perform quite well. As the amount of coding noise increases, the performance of the proposed solution decreases, while the strategy based on eigenalgorithms keeps the detection accuracy over 70 % even for QF values higher than 85. The improved performance of the eigenalgorithms-

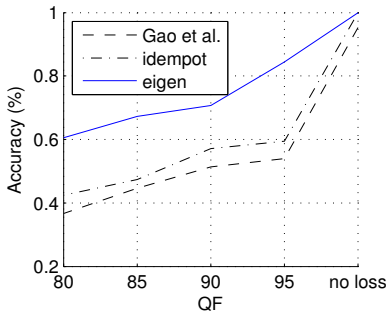

Fig. 5. Detection accuracy of different demosaicing detectors for different quantization settings in Scenario 1.

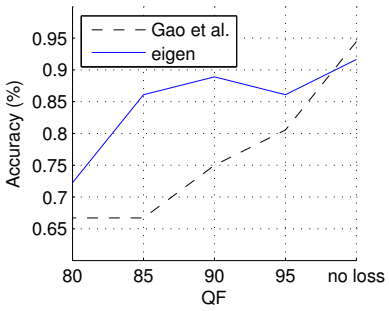

Fig. 6. Detection accuracy of different demosaicing detectors for different quantization settings in Scenario 2.

based approach can be explained considering that the energy of the compression noise is mainly located at high frequencies. By reinterpolating the signal, part of this energy is removed (since the interpolator is generally a low pass operator) leading to a less corrupted version of the image. This permits a more accurate detection. The detailed confusion matrices are reported at [25].

A second set of experiments was performed considering real cameras. To this purpose, a set of JPEG images was downloaded from the Dresden dataset [26] as in [20]. Four central areas of 512×512 pixels were used in this case (as described in [20]). Since the classification outcomes is found combining the classification results of these 4 images, the average precision of the different algorithms is a bit higher with respect to the first scenario (where a single feature array was computed on the whole image). Note also that image resolution is higher, and therefore, frequency spectra of coding blocks proves to fit a low-pass model better than images with smaller resolution. As a consequence, the amount of interpolation noise introduced by the different analysis algorithms is lower, leading to a more accurate identification. We downloaded images acquired with FujiFilm, Nikon Coolpix, and Nikon D70s cameras. The list of adopted images is available at [25]. In order to vary the amount of compression noise applied to images, we recompressed the decoded JPEG images with different quality factors QFs. Since a lot of additional noise sources (derived from the applied processing steps like white-balancing, gamma correction, etc.) affect the image, experimental results showed that using vectors of 5 features $\overline{p} = (p_A, p_B, p_C, p_D, p_E)$ permits an accurate characterization.

Each feature vector $\overline{p}$ is classified via a set of SVM classifiers (one per camera). Fig. 6 reports the detection results for the approach in [20] and the proposed one. Table 2 reports the complete confusion matrices obtained from uncompressed images and from images coded with QF=$90, 80$. All the data are available at [25]. It is possible to see that the robustness to compression is confirmed also in this case. The accuracy is higher than 80 % with $QF \geq 85$ for the eigenalgorithms-based approach, while the solution in [20] has a lower performance when strong compression is introduced. It is worth noticing that the performance of the algorithm in [20] is slightly better than the proposed solution whenever no compression is applied. This is due to the adoption of 69 feature values in place of the 5 feature values adopted by the eigenalgorithms-based approach.

Table 2. Confusion matrix for strategies eigen-based/Gao *et al.*.

	Fuji	**CoolPix**	**D70s**
Fuji	100.00/100.00	0.00/0.00	0.00/0.00
CoolPix	25.00/0.00	75.00/100.00	0.00/0.00
D70s	0.00/8.33	0.00/8.33	100.00/83.33

No loss

	Fuji	**CoolPix**	**D70s**
Fuji	100.00/91.67	0.00/0.00	0.00/8.33
CoolPix	33.33/25.00	66.67/41.67	0.00/33.33
D70s	0.00/8.33	0.00/0.00	100.00/91.67

QF=90

	Fuji	**CoolPix**	**D70s**
Fuji	91.67/91.67	8.33/0.00	0.00/8.33
CoolPix	33.33/33.33	66.67/16.67	0.00/50.00
D70s	0.00/8.33	0.00/0.00	100.00/91.67

QF=85

5. CONCLUSIONS

The paper presented a new strategy for the identification of the CFA interpolation strategy on static images that relies on reprocessing the analyzed image with some known demosaicing strategies, called "eigenalgorithms". The correlation between the obtained output and the original image under analysis permits identifying the original interpolation strategy with a nice accuracy ($>$ 80 %) even when the signal has been corrupted by compression noise. Future work will be devoted to investigate the influence of the number of features/eigenalgorithms on the detection performance. Moreover, we are planning to extend the approach to the identification of a wider set of algorithms in the presence of different noise sources. Preliminary results have shown that it is also possible to reverse the approach using the eigenalgorithms to generate forged images with consistent CFA-related footprints. Implementing this possibility, it will be possible to design antiforensic strategies for the synthesis of demosaicing algorithms that could be used to fool CFA-based camera detectors.

6. REFERENCES

[1] S. Milani, M. Fontani, P. Bestagini, M. Barni, A. Piva, M. Tagliasacchi, and S. Tubaro, "An overview on video forensic," *APSIPA Transactions on Signal and Information Processing*, vol. 1, no. 1, 2012.

[2] A. Piva, "An overview on image forensics," *ISRN Signal Processing*, vol. 2013, no. 496701, pp. 1–22, Jan. 2013.

[3] M. Chen, J. Fridrich, M. Goljan, and J. Lukás, "Source digital camcorder identification using sensor photo response nonuniformity," in *Proceedings of SPIE Electronic Imaging, Photonics West*, 2007.

[4] M. Kirchner, "Efficient estimation of CFA pattern configuration in digital camera images," in *Proceedings of SPIE Media Forensics and Security*, Jan. 2010, vol. 7541, pp. 754111–754111–12.

[5] W. Lu and Y.-P. Tan, "Color filter array demosaicking: new method and performance measures," *IEEE Transactions on Image Processing*, vol. 12, no. 10, pp. 1194–1210, Oct. 2003.

[6] A. Swaminathan, Min Wu, and K.J.R. Liu, "Nonintrusive component forensics of visual sensors using output images," *IEEE Transactions on Information Forensics and Security*, vol. 2, no. 1, pp. 91–106, Mar. 2007.

[7] H. Farid, "Digital Image Ballistic from JPEG Quantization," Department of Computer Science, Dartmouth College. Available on line, 2008.

[8] H. Cao and A.C. Kot, "Accurate detection of demosaicing regularity for digital image forensics," *IEEE Transactions on Information Forensics and Security*, vol. 4, no. 4, pp. 899–910, Dec. 2009.

[9] A. Swaminathan, Min Wu, and K.J.R. Liu, "Digital image forensics via intrinsic fingerprints," *IEEE Transactions on Information Forensics and Security*, vol. 3, no. 1, pp. 101–117, Mar. 2008.

[10] A. C. Gallagher and T. Chen, "Image authentication by detecting traces of demosaicing," in *Proceedings of IEEE Computer Vision and Pattern Recognition Workshops (CVPRW 2008)*, June 2008, pp. 1–8.

[11] A.E. Dirik and N. Memon, "Image tamper detection based on demosaicing artifacts," in *Proceedings of IEEE International Conference on Image Processing (ICIP 2009)*, Nov 2009, pp. 1497–1500.

[12] P. Bestagini, A. Allam, S. Milani, M. Tagliasacchi, and S. Tubaro, "Video codec identification," in *Proceedings of IEEE International Conference on Acoustics, Speech, and Signal Processing (ICASSP 2012)*, Mar. 2012, pp. 2257–2260.

[13] P. Bestagini, S. Milani, M. Tagliasacchi, and S. Tubaro, "Video codec identification extending the idempotency property," in *Proceedings of European Workshop on Visual Information Processing (EUVIP 2013)*, June 2013, pp. 220–225.

[14] S. Milani, M. Tagliasacchi, and S. Tubaro, "Identification of the motion estimation strategy using eigenalgorithms," in *Proceedings of IEEE International Conference on Image Processing (ICIP 2013)*, Sept. 15 – 18, 2013, pp. 4477 – 4481.

[15] Z. Zhu and T. Lin, "Idempotent H.264 intraframe multigeneration coding," in *Proceedings of the IEEE International Conference on Acoustics, Speech and Signal Processing (ICASSP 2009)*, april 2009, pp. 1033 –1036.

[16] G. Valenzise, V. Nobile, M. Tagliasacchi, and S. Tubaro, "Countering JPEG anti-forensics," in *Proceedings of the IEEE International Conference on Image Processing (ICIP 2011)*, 2011, pp. 1949–1952.

[17] M. Sorell, "Video provenance by motion vector analysis: A feasibility study," in *Proceedings of International Symposium on Communications Control and Signal Processing (ISCCSP 2012)*, May 2012, pp. 35–42.

[18] C.-C. Chang and C.-J. Lin, "LIBSVM: A library for support vector machines," *ACM Transactions on Intelligent Systems and Technology*, vol. 2, pp. 27:1–27:27, 2011, Software available at http://www.csie.ntu.edu.tw/ cjlin/libsvm.

[19] G. Schaefer and M. Stich, "UCID - An uncompressed colour image database," in *Proceedings of SPIE: Storage and Retrieval Methods and Applications for Multimedia*, Jan. 2004, vol. 5307, pp. 472 – 480.

[20] S. Gao, W. Hu, and R.-M. Hu, "Camera model identification based on the characteristics of CFA and interpolation," *Proceedings of International Conference on Digital-Forensics and Watermarking (IWDW 2011)*, vol. 7128, pp. 268–280, 2011.

[21] L. Zhang and X. Wu, "Color demosaicking via directional linear minimum mean square-error estimation," *IEEE Transactions on Image Processing*, vol. 14, no. 12, pp. 2167 – 2178, Dec. 2005.

[22] B. K. Gunturk, Y. Altunbasak, and R. M. Mersereau, "Color plane interpolation using alternating projections," *IEEE Transactions on Image Processing*, vol. 11, no. 9, pp. 997 – 1013, Sept. 2002.

[23] A. Buades, B. Coll, J.-M. Morel, and C. Sbert, "Self-similarity driven demosaicking," *Image Processing On Line*, 2011.

[24] S. Bayram, H. Sencar, and N. Memon, "Identifying digital camera using cfa interpolation," in *Advances in Digital Forensics II*, vol. 222, chapter 23, pp. 289 – 299. Boston: Springer, 2006.

[25] S. Milani, "Supporting material for CFA interpolation identification using eigenalgoriothms - http://www.dei.unipd.it/∼sim1mil/eigenCFA," 2013.

[26] T. Gloe and R. Böhme, "The 'Dresden Image Database' for benchmarking digital image forensics," in *Proceedings of the ACM Symposium on Applied Computing*, 2010, pp. 1584–1590.